Mine Water Environ (2016) 35:86–93
DOI 10.1007/s10230-015-0341-9

TECHNICAL COMMUNICATION

Hydrogeochemical Characteristics of Groundwater at the Xikuangshan Antimony Mine in South China

Tananga Mathews Nyirenda[1] · Jianwei Zhou[1] · Harold W.T. Mapoma[1] · Lina Xie[1] · Yi Li[1]

Received: 29 December 2014 / Accepted: 29 April 2015 / Published online: 12 May 2015

Abstract The hydrogeochemical influence of the Xikuangshan antimony mine on groundwater quality was investigated by analyzing groundwater from 24 springs in the area for major and trace elements. The samples had a pH of 7.6–8.5; total dissolved solids ranged from 125 to 607 mg/L. The groundwater was dominated by alkaline earths ($Ca^{2+} + Mg^{2+}$) over the alkalies ($Na^{+} + K^{+}$), and weak acids (HCO_3^-) over strong acids ($SO_4^{2-} + Cl^-$). Calcite was generally supersaturated and gypsum was always undersaturated, while dolomite was undersaturated in 34 % of the samples. Iron was negatively correlated with Ca^{2+}, Mg^{2+}, and SO_4^{2-}, which is consistent with Fe removal during acid buffering. Scatter diagrams and correlation coefficients between the major ions indicate dissolution of carbonates and gypsum as major processes, which could promote calcite precipitation.

Keywords Water–rock interactions · Gypsum dissolution · Carbonates · Acid buffering · Mining

Introduction

Antimony (Sb) is an important metalloid mined in more than 15 countries in the world, with China accounting for over 80 % of the world's mined production and most of the reserve base (He et al. 2012). The Xikuangshan (XKS) Sb mine, located in Hunan province, China, is the largest Sb mine in the world (Peng et al. 2003). The most serious environmental concern associated with mining is acid mine drainage (AMD) and its potential impact on groundwater resources (Gass 2012). Mine water mitigation and management takes different forms, and it is important to understand the hydrogeochemical processes that occur during and after AMD formation (Gomo and Vermeulen 2014). The evolving hydrochemical groundwater type depends on the chemistry of the water and the geochemical processes that take place in the subsurface (Rajmohan and Elango 2004). We used a diagnostic approach to investigate the hydrogeochemical characteristics of groundwater at the XKS Mine, applying scatter plots, the USGS geochemical code PHREEQC (Parkhurst and Appelo 2013), and Piper diagrams as complementary tools to analyze its chemistry, as suggested by Han et al. (2013) and Gomo and Vermeulen (2014).

Methods and Materials

Study Area Description and Geology

The XKS Sb mine is situated northeast of Lenshuijiang city at 27.7°N and 111.4°E (Fig. 1). It hosts several ore-grade stibnite deposits and still has reserves of 40 million t after 110 years of exploitation (Qi et al. 2011). The study area has a subtropical, monsoon climate with an annual average

Electronic supplementary material The online version of this article (doi:10.1007/s10230-015-0341-9) contains supplementary material, which is available to authorized users.

✉ Jianwei Zhou
jw.zhou@cug.edu.cn

Tananga Mathews Nyirenda
tananganyirenda@yahoo.com

[1] School of Environmental Studies, China University of Geosciences (Wuhan), Lumo Rd 388, Wuhan 340074, Hubei, People's Republic of China

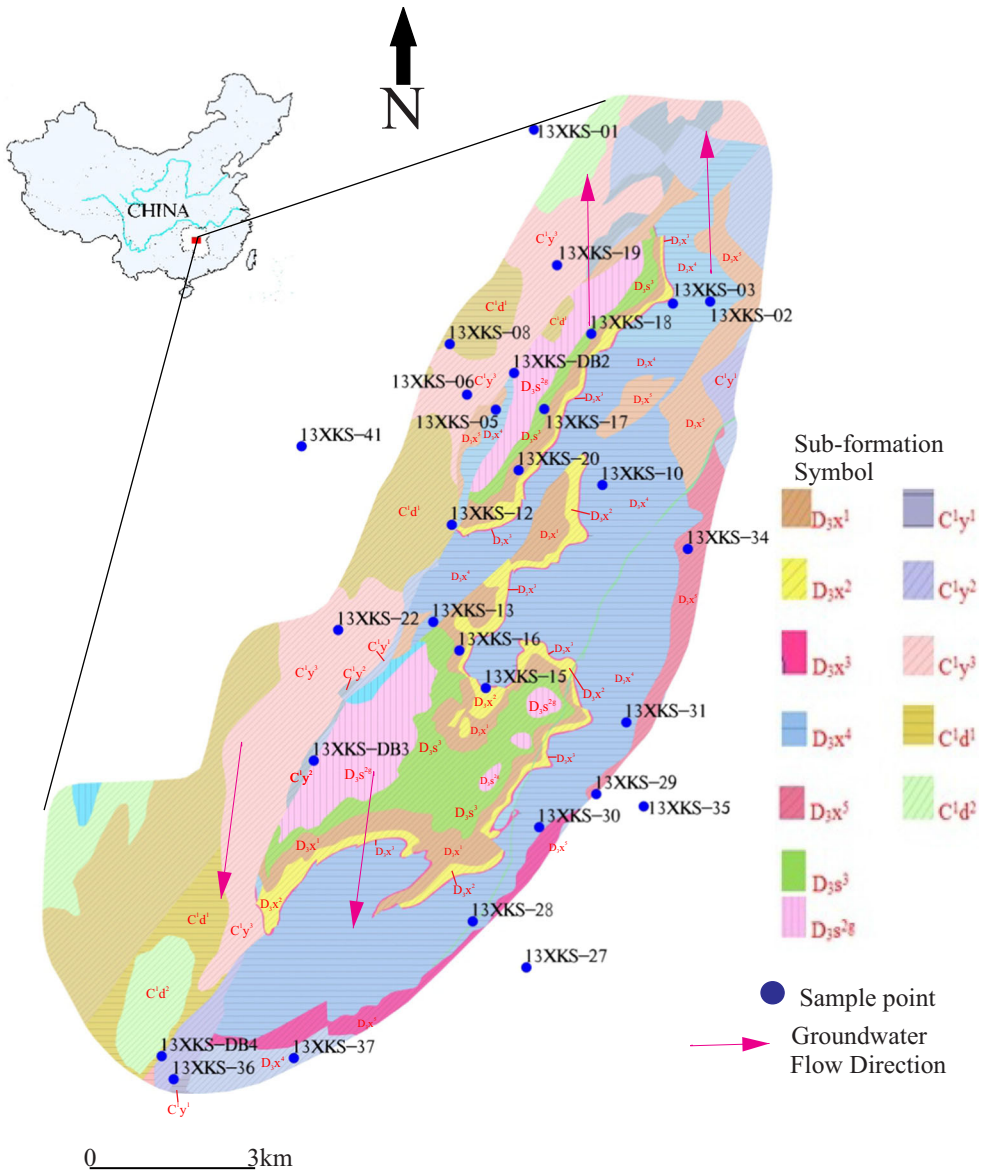

Fig. 1 Sketch map showing the location of the XKS Sb mine and the sampling points

precipitation of 1457.0 mm. Average relative humidity is 53.1 %, with a mean annual temperature of 16.8 °C, normally ranging between 4.9 °C (January) and 28.2 °C (July).

The deposit is located at the intersection between the NNE-trending Chengbu–Xinhua fault, and the NW-trending Shuangfeng-XKS fault (Fan et al. 2004). The Upper Devonian Shetianqiao (D_3s) and XKS (D_3x) Formations occur in the core of the anticline, surrounded by the Lower Carboniferous Yanguan (C_{1y}) and Datang (C_{1d}) Formations (Peng et al. 2003). The XKS Sb deposit is hosted by dark gray chert in the black shale series of the Upper Devonian Shetianqiao Formation. The Shetianqiao Formation is enriched in Sb, and contains many small Sb deposits in addition to the XKS deposit, while the Pre-Devonian rocks and the Upper Devonian rocks that host the ores contain abundant Sb and may have supplied Sb for the ore deposits (Fan et al. 2004). The exposed strata are predominantly carbonates, locally interbedded with sandstone, marlstone, and shale. Trace amounts of pyrite, pyrrhotite, and sphalerite occur in the ore along with the primary gangue minerals, quartz and calcite, and secondary barite and fluorite (Fan et al. 2004). Based on the lithofacies analyses for the XKS sections, five facies associations can be outlined, including inner ramp peritidal, inner ramp organic bank and mound, mid ramp, outer ramp, and shelf basin facies associations (Shao et al. 2011). The peritidal platform facies is characterized by dolomite, gypsum, and anhydrite beds.

The carbonaceous rocks contain 15–35 ppm of Sb, compared to the average Sb content of 0.2–0.5 ppm in the earth's crust, while the rocks of the broad region around XKS contain ≈6 ppm of Sb (Ottens 2007). Ore textures in the XKS mine range from massive to disseminated, and from drusy to coarsely crystalline, with stibnite (Sb_2S_3) being the only ore mineral (He 2007). The stibnite occurs as columnar and radiating aggregates distributed in a dark–gray chert (Fan et al. 2004). The XKS ores can be divided into four types: quartz–stibnite, calcite–stibnite, barite–quartz–stibnite, and fluorite–quartz–stibnite. The first two types are the most important and constitute 90 % of the XKS reserves. The XKS ores are characterized by a very high Sb content; the annual production capacity of the mine is 55,000 t of ores, 40,000 t of Sb products, and 40,000 t of zinc (Zn) ingots (Liu et al. 2011).

Sampling

A total of 24 groundwater samples were collected from springs representing different aquifers (Table 1) in the XKS mine area in July 2013 and analyzed in August 2013. Samples were collected in polyethylene bottles, while pH and Eh were measured in the field at each sampling point. Water samples for major and trace element analysis were filtered immediately after collection through 0.45 μm Millipore filters into 50 mL washed high density polyethylene (HDPE) bottles. Water samples for cation analysis were acidified to pH < 2 with HNO_3 (2 %) and refrigerated until laboratory analyses could be completed.

Chemical Analysis and Calculations

All samples were analyzed at the China University of Geosciences (Wuhan). The samples were analyzed by ultraviolet–visible spectroscopy (UV–Vis) for SO_4^{2-}, Cl^-, and F^-. Bicarbonates $\left(HCO_3^-\right)$ were measured by titration. Inductively coupled plasma—optical emission spectrometry (ICAP6300) was used to analyze Ca^{2+}, Mg^{2+}, Al^{3+}, Na^+, and K^+. An atomic fluorescence spectrometer (AFS-820) was used to analyze Fe, As, and Sb. The total dissolved solids (TDS) was computed as the sum of ions for each sample using USGS method I-1751-85 (Fishman and Friedman 1989). In this method, the concentrations of all determined constituents were treated as reported by the analysis, with the exception of HCO_3^-, which is assumed to

Table 1 Detailed information for water sampling sites at Xikuangshan Sb mine area

Sample ID	Source of water	Symbol of sub-formation	Name of formation	Lithology
13XKS-01	Spring	C_1d^2	Datang formation	Carboniferous sandstone
13XKS-02	Spring	D_3x^4	Xikuangshan formation	Massive limestone
13XKS-03	Spring	D_3x^4	Xikuangshan formation	Massive limestone
13XKS-05	Spring	D_3x^4	Xikuangshan formation	Massive limestone
13XKS-06	Spring	C_1y^3	Yanguan formation	Carboniferous limestone
13XKS-08	Spring	C_1d^1	Datang formation	Carboniferous sandstone
13XKS-12	Spring	D_3x^1	Xikuangshan formation	Calcareous shale
13XKS-13	Spring	D_3x^1	Xikuangshan formation	Calcareous shale
13XKS-15	Spring	D_3x^3	Xikuangshan formation	Shale + bedded hematite
13XKS-17	Spring	D_3x^1	Xikuangshan formation	Calcareous shale
13XKS-18	Spring	D_3x^1	Xikuangshan formation	Calcareous shale
13XKS-19	Spring	C_1y^3	Yanguan formation	Carboniferous limestone
13XKS-20	Spring	D_3x^2	Xikuangshan formation	Shale
13XKS-22	Spring	C_1y^3	Yanguan formation	Carboniferous limestone
13XKS-27	Spring	D_3x^5	Xikuangshan formation	Shale + marl + sandstone
13XKS-28	Spring	D_3x^4	Xikuangshan formation	Massive limestone
13XKS-29	Spring	D_3x^5	Xikuangshan formation	Shale + marl + sandstone
13XKS-30	Spring	D_3x^5	Xikuangshan formation	Shale + marl + sandstone
13XKS-31	Spring	D_3x^5	Xikuangshan formation	Shale + marl + sandstone
13XKS-34	Spring	D_3x^5	Xikuangshan formation	Shale + marl + sandstone
13XKS-35	Spring	C_1y^2	Yanguan formation	Carboniferous limestone
13XKS-36	Spring	C_1y^2	Yanguan formation	Carboniferous limestone
13XKS-37	Spring	D_3x^4	Xikuangshan formation	Massive limestone
13XKS-41	Spring	C_1d^1	Datang formation	Carboniferous sandstone

exist as carbonate (e.g. $CaCO_3$) in the residue on evaporation (Eq. 1).

$$2HCO_3^- = CO_3^{2-} + CO_2 + H_2O \quad (1)$$

Therefore, the bicarbonate in solution was mathematically converted to its equivalent weight as carbonate in the residue, as shown in Eq. 2.

$$\text{mg/L } CO_3^{2-} = \frac{\text{mg/L } HCO_3^-}{2.03} \quad (2)$$

Saturation indices (SI) for the mineral phases were calculated using PHREEQC (Parkhurst and Appelo 2013). A positive SI indicates that the water is supersaturated with respect to a particular mineral phase, while a negative SI indicates undersaturation and potential for dissolution (Pérez-López et al. 2007). Scatter diagrams and Pearson product moment (PPM) correlation coefficients between chemical ion concentrations were plotted and calculated respectively using Microsoft Office Excel 2007 spreadsheets. The Piper diagram was produced using GW_Chart version 1.26.0.0 (http://water.usgs.gov/nrp/gwsoftware/GW_Chart/GW_Chart.html).

Results and Discussion

The geochemical analysis of the groundwater samples are given in Table 2. The pH of the water ranged from 7.6 to 8.5, with a mean value of 7.9, indicating alkaline mine water. The total dissolved solids (TDS) ranged between 187 and 1360 mg/L, with an average of 498 (Table 2). This spatial variation in TDS values was attributed to variations in lithology, hydrological processes, and prevailing mining activities (Zakir et al. 2013). The average major ions concentrations in all of the groundwater followed the order; $HCO_3^- > SO_4^{2-} > Ca^{2+} > Cl^- > Na^+ > Mg^{2+} > K^+ > F^-$. The groundwater samples showed dominance of alkaline earths ($Ca^{2+} + Mg^{2+}$) over the alkalies ($Na^+ + K^+$), and weak acids (HCO_3^-) over strong acids $(SO_4^{2-} + Cl^-)$. The Piper diagram (Fig. 2) classified the spring samples as Ca–HCO_3–SO_4 type waters in 66 % of the sampling points, and Ca–SO_4–HCO_3 type waters in the remaining sampling points. These water types, considered with the alkaline pH, imply that the carbonate rocks were able to neutralize any acidity derived from oxidation of sulfide minerals associated with the Sb mine.

Saturation Indices

Groundwater of the Ca–HCO_3–SO_4 and Ca–SO_4–HCO_3 type, with minor Mg^{2+}, suggests that calcium carbonate minerals, such as calcite and, to a lesser extent, dolomite, could be buffering AMD from the mine area. However, gypsum dissolution, which would contribute equal moles of Ca^{2+} and SO_4^{2-} (Li et al. 2013), could also produce this water quality; hence, understanding the SI values of calcite, dolomite, and gypsum is important.

The SI value of calcite and dolomite ranged from −0.44 to 0.90 (mean = 0.51) and from −1.65 to 0.86 (mean = 0.06), respectively (Table 2). Despite this, a substantial number of SI results for dolomite (34 %) and calcite (4 %) were negative, indicating that dolomite and calcite were undersaturated in those samples and could continue to dissolve if present along the groundwater flow path, even though the groundwater was, in general, saturated with calcite. Furthermore, calcite and dolomite SI values followed a positive linear trend that was characterized by a correlation coefficient of 0.95 (Fig. 3). This showed that the mineral phases were changing similarly, which is evidence that the reactions of the two minerals are controlled by a similar hydrogeochemical process (AMD-calcite and -dolomite buffering). The SI of gypsum ranged from −2.26 to −0.91 (mean = −1.56, Table 2), suggesting that the groundwater would also tend to dissolve gypsum if present along the flow path.

However, the calcite and dolomite SI values did not correlate with TDS (Fig. 4). Additionally the concentrations of Ca^{2+}, Mg^{2+}, and HCO_3^- did not correlate with $SI_{calcite}$ and $SI_{dolomite}$ (Fig. 5). This suggests that calcite and dolomite did not continue to dissolve, and may have precipitated where supersaturation was indicated. The inverse relation between ion concentration and SI for calcite and dolomite at SI > 0.5 is consistent with ion precipitation.

In contrast, the SI_{gypsum} was negative, and was positively correlated with TDS (Fig. 4). This indicates that the groundwater has the capacity to dissolve gypsum, which could explain the observed supersaturation of calcite. Continued gypsum dissolution could explain the increases in Ca^{2+} and SO_4^{2-} concentrations in the XKS groundwater, despite the potential for carbonate mineral precipitation.

Hydrogeochemical Processes

The evolving hydrochemical groundwater type depends on water chemistry as well as the different geochemical processes that take place in the subsurface (Rajmohan and Elango 2004). Since our study was investigating AMD-influenced hydrogeochemical processes, measured metal concentrations were used to corroborate these expectations. AMD generation in the XKS mining environment is generally determined by the oxidation of metal sulfides, especially pyrite (FeS_2) and pyrrhotite ($Fe_{1-x}S$), which are found with the Sb ore in trace amounts (Fan et al. 2004).

Table 2 Geochemical characteristics of groundwater from XKS Sb mine

Parameter	PH	K^+ (mg/l)	Na^+ (mg/l)	Ca^{2+} (mg/l)	Mg^{2+} (mg/l)	Cl^- (mg/l)	SO_4^{2-} (mg/l)	F^- (mg/l)	HCO_3^- (mg/l)	TDS (mg/l)	Calcite (SI)	Dolomite (SI)	Gypsum (SI)
13XKS-01	7.84	1.42	3.2	100	11.7	9.88	117	0.02	226	354	0.54	0.35	−1.40
13XKS-02	8.08	0.4	0.75	41.7	2.26	5.32	25	0.02	101	125	0.15	−0.76	−2.26
13XKS-03	8.01	0.71	10.7	58	9.71	5.32	86.1	0.60	142	241	0.31	0.05	−1.68
13XKS-05	7.95	0.7	2.77	59.1	5.69	5.32	83.3	0.11	107	210	0.15	−0.52	−1.67
13XKS-06	8.06	0.68	2.15	104	5.08	6.08	88.9	0.02	233	322	0.79	0.49	−1.48
13XKS-08	7.97	0.46	1.71	88.4	5.08	6.08	61.1	0.02	224	273	0.64	0.25	−1.68
13XKS-12	8.34	0.52	1.8	89.2	4.33	5.32	75	0.02	171	260	0.88	0.66	−1.59
13XKS-13	7.70	1.31	27.3	150	10.8	15.2	283	0.70	217	596	0.49	0.04	−0.94
13XKS-15	7.87	0.44	1.3	94	4.21	5.32	80.6	0.02	212	290	0.54	−0.07	−1.54
13XKS-17	7.92	5.77	41.8	82.1	10.9	18.2	158	0.72	182	407	0.42	0.18	−1.35
13XKS-18	8.00	1.54	1.31	52.6	2.05	5.32	61.1	0.62	77.8	163	0.03	−1.14	−1.82
13XKS-19	7.61	3.43	4.19	56.4	5.83	7.6	108	0.28	64.1	218	−0.44	−1.65	−1.58
13XKS-20	7.65	7.03	16.3	106	8.05	19	175	0.56	165	413	0.22	−0.47	−1.21
13XKS-22	7.93	1.57	29	122	6.69	19	194	0.88	223	483	0.67	0.28	−1.14
13XKS-27	8.07	0.55	1.72	45.7	4.25	6.84	38.9	0.02	96.1	145	0.14	−0.54	−2.06
13XKS-28	8.27	0.49	1.17	73.4	3.19	7.6	52.8	0.02	168	221	0.75	0.34	−1.79
13XKS-29	7.72	0.24	3.59	113	2.88	11.4	69.4	0.02	270	334	0.56	−0.26	−1.55
13XKS-30	7.98	0.86	5.75	158	19.3	11.4	297	0.40	221	602	0.78	0.86	−0.91
13XKS-31	7.85	1.46	14.6	148	22	7.6	294	0.70	241	607	0.67	0.71	−0.94
13XKS-34	7.94	0.97	3.05	115	6.81	6.84	88.9	0.02	272	355	0.78	0.54	−1.46
13XKS-35	8.32	0.5	0.67	81.6	3.99	5.32	44.4	0.02	197	233	0.90	0.70	−1.83
13XKS-36	7.93	0.2	0.74	113	6.82	5.32	83.3	0.02	276	346	0.77	0.53	−1.49
13XKS-37	8.47	0.2	0.93	65.4	4.06	5.32	41.7	0.02	151	192	0.85	0.71	−1.92
13XKS-41	8.11	0.32	0.55	68.9	3.57	3.8	27.8	0.02	198	203	0.65	0.22	−2.08

The high proportion of SO_4^{2-} (Table 2) in indicative of sulfide mineral oxidation. The overall FeS_2 oxidation reaction produces 4 mol of H^+ for each mole of FeS_2 oxidized and 2 mol of SO_4^{2-} (Eq. 3).

$$FeS_2 + 3.75O_{2(aq)} + 1.5H_2O \leftrightarrow Fe(OH_{3(s)}) + 2SO_4^{2-} + 4H^+ \quad (3)$$

Despite the natural oxidation process that produces acidity, the quality of the drainage emerging from a mine largely depends on whether minerals are present that are capable of neutralizing the acidic water. Given the measured pH at the XKS mine, it was expected that calcite ($CaCO_3$) was the main carbonate controlling buffering reactions as it is dominant in the pH range of 6.5–7.5, releasing Ca^{2+}. Iron shows a weak negative correlation with Ca^{2+}, Mg^{2+} and SO_4^{2-} (Fig. 6), which is consistent with Fe removal during neutralization of AMD by carbonates.

However, it is worth noting that FeS_2 buffering by calcite is not the only source of SO_4^{2-} and Ca^{2+} in groundwater. If Ca^{2+} and SO_4^{2-} were derived solely from gypsum dissolution, the ratio of $[Ca^{2+}]/[SO_4^{2-}]$ would be 1:1; however the ratio of $[Ca^{2+}] : [SO_4^{2-}]$ is 1.75 (Supplementary Fig. 1). Presuming that gypsum dissolution takes place, ion exchange or calcium dissolution are consistent with the observed $[Ca^{2+}] : [SO_4^{2-}]$ ratio being more than 1:1 (Han et al. 2013). This suggests that there are other sources of SO_4^{2-} and Ca^{2+}, apart from gypsum, with the most likely being the FeS_2-carbonate reactions.

To confirm this, measured metal concentrations from the XKS mine groundwater were used to validate the overall reactions involving the oxidation of and neutralization by calcite, which could yield $[Ca^{2+}] : [SO_4^{2-}]$, ranging from 1:1 to 2:1, as indicated by reactions 4 and 5 (Han et al. 2013).

$$FeS_2 + 2CaCO_3^- + 3.5O_2 + H_2O = Fe^{2+} + 2SO_4^{2-} + 2Ca^{2+} + 2HCO_3^- \quad (4)$$

$$FeS_2 + 4CaCO_3^- + 3.75O_2 + 3.5H_2O = Fe(OH)_3 + 2SO_4^{2-} + 4Ca^{2+} + 4HCO_3^- \quad (5)$$

The ratio of $[Ca^{2+}] : [SO_4^{2-}]$ is 1.75 (Supplementary Fig. 1), which is consistent with reactions 4 and 5 (correlation = 0.81). Calcite is not the only carbonate source of

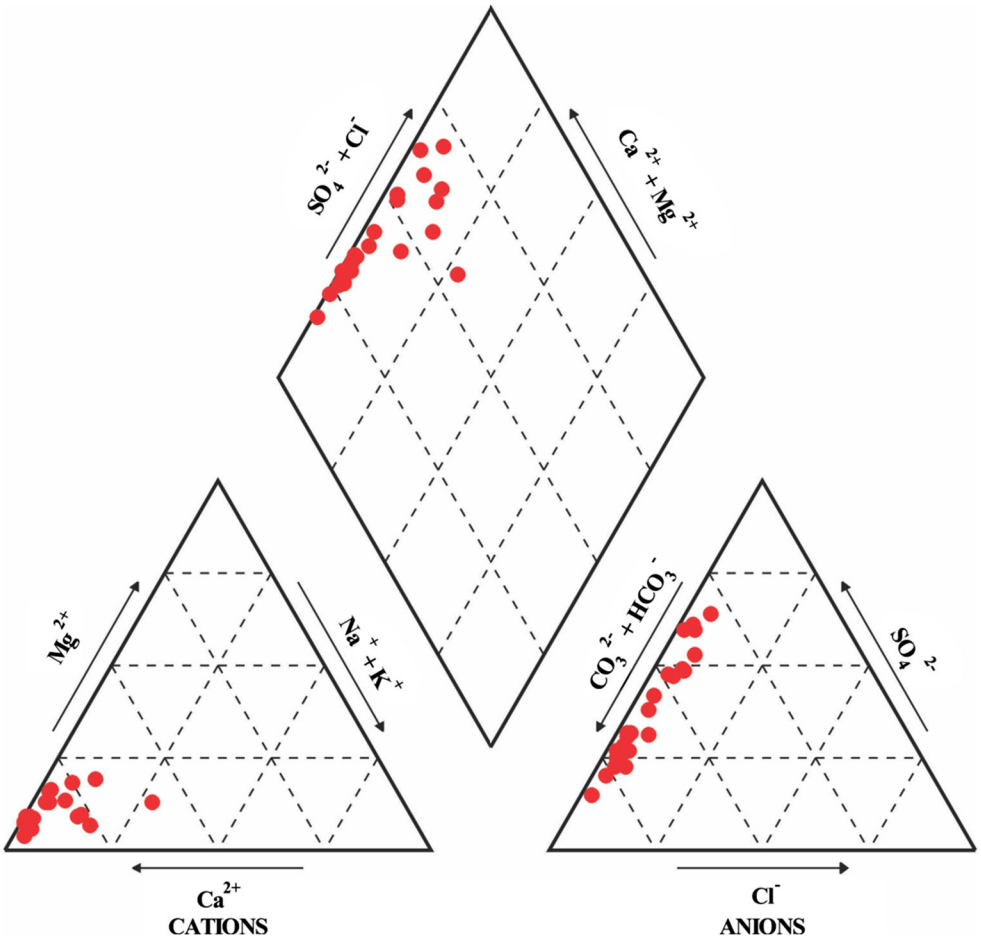

Fig. 2 Piper diagram of groundwater samples from the XKS Sb mine area

Ca^{2+}; dolomite can be another source. If calcite was the sole source of Ca^{2+} and HCO_3^-, the slope for $[Ca^{2+}]/[HCO_3^-]$ would be 1:1– 1:2, as indicated by Eqs. 6 and 7. The dissolution of calcite at pH < 5 depends solely on the pH (Eq. 6), while dissolution at pH > 5 occurs as indicated by Eq. 7 (Plummer et al. 1979).

$$CaCO_3^- + H^+ = Ca^{2+} + HCO_3^- \quad (6)$$

$$CaCO_3^- + H_2O + CO_2 = Ca^{2+} + 2HCO_3^- \quad (7)$$

The concentration of Ca^{2+} increases with that of HCO_3^- (Supplementary Fig. 1), with a slope of 1.9, which exceeds the range for $[Ca^{2+}/HCO_3^-]$ of 1:1–1:2 indicated by Eqs. 6 and 7. Furthermore, the concentration of HCO_3^- increases as TDS increases (Supplementary Fig. 2), but the SI for calcite >0, indicating that calcite dissolution is not a feasible source. (Please note that supplementary files accompany the on-line version of this paper, which can be downloaded for free by all journal subscribers and IMWA members.) Similarly, the SI_{mean} for dolomite was >0, even though some SI readings (34 %) for dolomite were <0, indicating that dolomite was still a source of Ca^{2+} and Mg^{2+}. The sum of Ca^{2+} and Mg^{2+} increases with HCO_3^- (Supplementary Fig. 3), which indicates that dolomite dissolution may be an additional source of the increased Ca^{2+} in the XKS groundwater. Dolomite dissolution is slower than calcite dissolution, so groundwater may be saturated with calcite while undersaturated with dolomite (Han et al. 2013).

The $([Ca^{2+}] + [Mg^{2+}]) : [HCO_3^-]$ ratio for the groundwater at the XKS mine was >2 (Supplementary Fig. 4), which is greater than the expected mole ratio $([Ca^{2+}] + [Mg^{2+}]) : [HCO_3^-]$ of 1:1–1:2 for the dissolution of calcite and dolomite. Although dolomite is the most likely source of Mg^{2+}, the mole ratio of $[Ca^{2+}]$:$[Mg^{2+}]$ in the XKS groundwater is substantially >1 (Supplementary Fig. 11), which indicates that dolomite dissolution is not an important source of Ca^{2+}. Additionally Mg concentrations are relatively minor, which implies that dolomite dissolution is a minor reaction. From earlier analysis, it can be seen that neutralization of sulfuric acid by calcite combined with gypsum dissolution are the main sources of the alkaline pH and elevated concentrations of Ca^{2+} and SO_4^{2-} in the XKS groundwater.

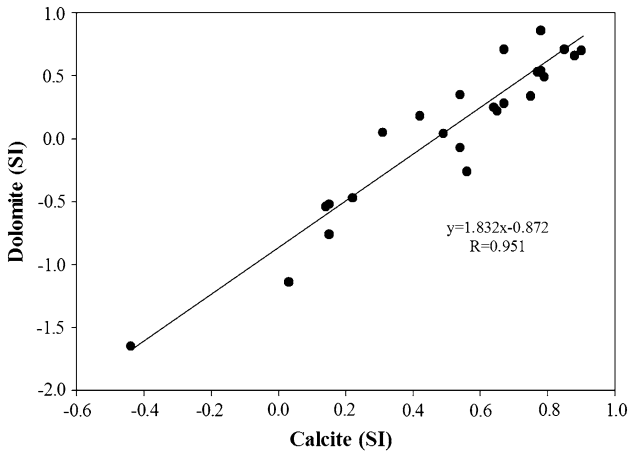

Fig. 3 Plot of SI dolomite versus SI calcite

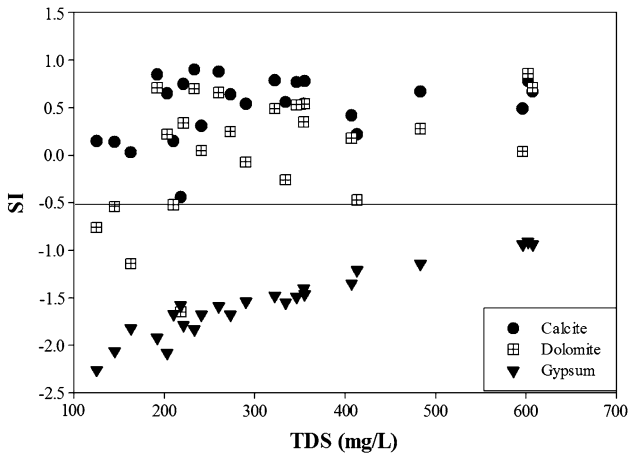

Fig. 4 Scatter plot of TDS versus SI

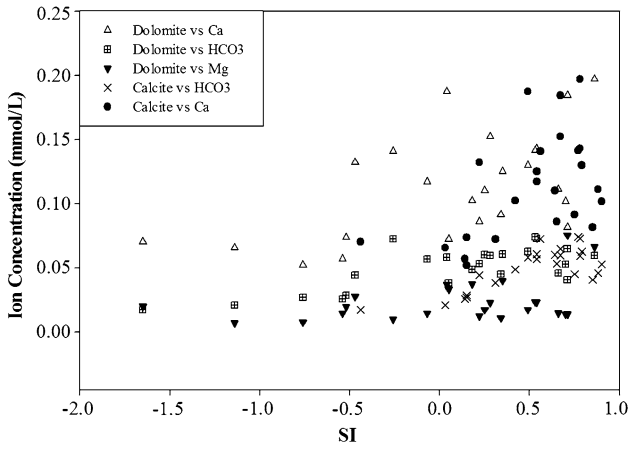

Fig. 5 Plot of SI (calcite and dolomite) versus ion concentration

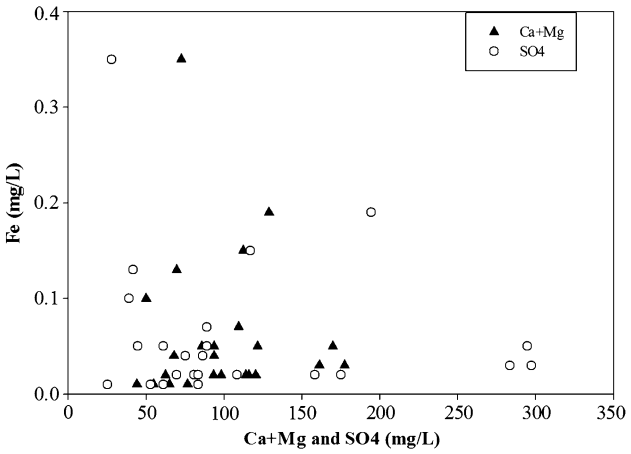

Fig. 6 Plot of $Ca^{2+} + Mg^{2+}$ and SO_4^{2-} versus Fe

Conclusion

This paper describes AMD-influenced groundwater and hydrogeochemical processes contributing to the groundwater characteristics at the XKS Sb mine. Pyrite and associated sulfide minerals associated with the Sb ore are potential sources of acidity, whereas carbonate minerals in the host rocks are potential sources of neutralization. The XKS Sb mine is mainly characterized by alkaline pH groundwater of Ca–HCO_3–SO_4 and Ca–SO_4–HCO_3 hydrochemical groundwater types. To obtain the type waters with an alkaline pH, both gypsum and calcite dissolution (neutralization) probably occurred. The host rocks have been described as calcareous, so the presence of calcite is assumed. Calcite would tend to dissolve until reaching saturation ($SI_{calcite=0}$), after which gypsum dissolution would increase the concentration of calcium and promote supersaturation with calcite. The groundwater showed dominance of alkaline earths over the alkalies, and weak acids over strong acids. The SI values for calcite and dolomite indicate that most samples were supersaturated with the carbonate minerals, whereas gypsum was undersaturated and hence still capable of dissolving. Thus, it can be concluded that the major water–rock interactions that explain the geochemical evolution of the groundwater are the dissolution of calcite, dolomite, and gypsum. Groundwater chemistry from the XKS Sb mine area indicates high concentrations of HCO_3^- and Ca^{2+}, suggesting that calcite is buffering the acidity released by the oxidation of iron sulfides in the ore body. However, continued increases of SO_4^{2-} and Ca^{2+} after the water was saturated with calcite resulted from the gypsum dissolution. The slope of

$\left(\left[Ca^{2+}\right]+\left[Mg^{2+}\right]\right)/\left[HCO_3^-\right]$ exceeds that of carbonate mineral dissolution because of the addition of Ca^{2+} from gypsum dissolution and, consequently, the removal of Ca^{2+}, Mg^{2+} and HCO_3^- by carbonate mineral precipitation. This information on the hydrochemical evolution of groundwater is important for those responsible for managing the groundwater associated in the XKS mine area.

References

Fan D, Zhang T, Ye J (2004) The XKS Sb deposit hosted by the Upper Devonian black shale series, Hunan, China. Ore Geol Rev 24(1–2):121–133. doi:10.1016/j.oregeorev.2003.08.005

Fishman MJ, Friedman LC (eds) (1989) Solids, sum of constituents, calculation; methods for determination of inorganic substances in water and fluvial sediments. USGS Techniques WRI Report 5-A1, p 459–460, http://pubs.usgs.gov/twri/twri5-a1/pdf/TWRI_5-A1.pdf

Gass K (2012) Acid mine drainage: can we fix the mess? World Pumps 2012(3):24–27. doi:10.1016/S0262-1762(12)70063-9

Gomo M, Vermeulen D (2014) Hydrogeochemical characteristics of a flooded underground coal mine groundwater system. J Afr Earth Sci 92(2014):68–75. doi:10.1016/j.jafrearsci.2014.01.014

Han Y, Wang G, Cravotta CA, Hu W, Bian Y, Zhang Z, Liu Y (2013) Hydrogeochemical evolution of Ordovician limestone groundwater in Yanzhou, North China. Hydrol Process 27(16):2247–2257. doi:10.1002/hyp.9297

He M (2007) Distribution and phytoavailability of antimony at an antimony mining and smelting area, Hunan, China. Environ Geochem Health 29(3):209–219. doi:10.1007/s10653-006-9066-9

He M, Wang X, Wu F, Fu Z (2012) Antimony pollution in China. Sci Total Environ 421–422:41–50. doi:10.1016/j.scitotenv.2011.06.009

Li P, Qian H, Wu J, Zhang Y, Zhang H (2013) Major ion chemistry of shallow groundwater in the Dongsheng Coalfield, Ordos Basin, China. Mine Water Environ 32(3):195–206. doi:10.1007/s10230-013-0234-8

Liu B, Wu F, Li X, Fu Z, Deng Q, Mo C, Zhu J, Zhu Y, Liao H (2011) Arsenic, antimony and bismuth in human hair from potentially exposed individuals in the vicinity of antimony mines in Southwest China. Microchem J 97(1):20–24. doi:10.1016/j.microc.2010.07.008

Ottens B (2007) Chinese stibnite: Xikuangshan, Lushi, Wuning and other localities. Miner Rec 38(1):3–17

Parkhurst DL, Appelo CAJ (2013) Description of input and examples for PHREEQC version 3—a computer program for speciation, batch-reaction, one-dimensional transport, and inverse geochemical calculations. USGS Techniques Methods 6-A43, http://pubs.usgs.gov/tm/06/a43

Peng JT, Hu RZ, Burnard PG (2003) Samarium–neodymium isotope systematics of hydrothermal calcites from the Xikuangshan antimony deposit (Hunan, China): the potential of calcite as a geochronometer. Chem Geol 200(1–2):129–136. doi:10.1016/S0009-2541(03)00187-6

Pérez-López R, Nieto JM, De Almodóvar GR (2007) Utilization of fly ash to improve the quality of the acid mine drainage generated by oxidation of a sulphide-rich mining waste: column experiments. Chemosphere 67(8):1637–1646. doi:10.1016/j.chemosphere.2006.10.009

Plummer LN, Parkhurst DL, Wigley TML (1979) Critical review of kinetics of calcite dissolution and precipitation. In: Jenne EA (Ed) Chemical Modeling in Aqueous Systems, Speciation, Sorption, Solubility and Kinetics. Am Chem Soc Symp Ser 93:537–573

Qi C, Wu F, Deng Q, Liu G, Mo C, Liu B, Zhu J (2011) Distribution and accumulation of antimony in plants in the super-large Sb deposit areas, China. Microchem J 97(1):44–51. doi:10.1016/j.microc.2010.05.016

Rajmohan N, Elango L (2004) Identification and evolution of hydrogeochemical processes in the groundwater environment in an area of the Palar and Cheyyar River Basins, Southern India. Environ Geol 46(1):47–61. doi:10.1007/s00254-004-1012-5

Shao L, Wang D, Cai H, Wang H, Lu L, Zhang P (2011) Ramp facies in an intracratonic basin: a case study from the Upper Devonian and Lower Carboniferous in central Hunan, southern China. Geosci Front 2(3):409–419. doi:10.1016/j.gsf.2011.06.003

Zakir HM, Islam MM, Arafat MY, Sharmin S (2013) Hydrogeochemistry and quality assessment of waters of an open coal mine area in a developing country: a case study from Barapukuria, Bangladesh. Int J Geosci Res 1:20–44